

Relativistic time delay analysis of pulsar signals near ultra-compact objects

Viraj Kalsariya,^{1,*} Parth Bambhaniya,^{1,†} and Pankaj S. Joshi^{1,‡}

¹*International Center for Space and Cosmology, Ahmedabad University, Ahmedabad 380009, Gujarat, India*

The upcoming discoveries of pulsars orbiting the center of the Milky Way will present unparalleled opportunities to examine the causal structure of the spacetime geometry of Sagittarius A*. In this paper, we investigate the fully relativistic propagation time delay of pulsar signals in the Joshi-Malafarina-Narayan (JMN-1) and Janis-Newman-Winicour (JNW) spacetimes. This delay arises basically from the spacetime curvatures in the vicinity of these ultra-compact objects, induced by the intense gravitational field near the Galactic Center (GC). Using the principles of gravitational lensing, we compute the arrival time of photons originating from a pulsar in orbit around the GC. To validate our approach, we compare our time delay analysis of the Schwarzschild black hole with the corresponding delay in the post-Newtonian framework. Subsequently, we find that the propagation time of pulsar signal is greater and lesser for the given horizon-less ultra-compact objects for direct and indirect propagation respectively. Therefore, our results suggest quite significant propagation time delay differences in JMN-1 and JNW spacetimes, when compared to the Schwarzschild black hole case. This can be inferred as a possible distinguishing feature for these ultra-compact objects' geometries.

Keywords: Astrophysical black holes, Ultra-compact Objects, Milky Way Galactic Center, Pulsars, Time delay

I. INTRODUCTION

In 1939, Oppenheimer, Snyder, and Datt (OSD) introduced a collapse model, which is a solution for the dynamical collapse of a spherically symmetric, homogeneous dust cloud [1, 2]. This model assumed ideal conditions, such as uniform density within the collapsing star and zero gas pressure, simplifying the Einstein equations. This model essentially hinted at the black hole formation as the final fate of continued collapse, with a spacetime singularity at the center, hidden within an event horizon. Based on the OSD model, later in 1969, Penrose proposed the Cosmic Censorship Conjecture (CCC) suggesting that space-time singularities must remain hidden from distant observers when a massive star gravitationally collapses [3].

However, due to highly ideal assumptions used in the OSD model, the question of the final fate of collapse remained open under physically more realistic conditions. While the CCC implies that gravitational collapse must lead exclusively to black holes only, subsequent research highlighted that an inhomogeneous matter collapse, for

example with density higher at the center and decreasing slowly as we move away, can result in naked singularities [4–7]. In this latter case, the spacetime singularity forming as a collapse final state is no longer hidden within an event horizon of gravity. This highlights the importance of considering various initial conditions in gravitational collapse scenarios, as they dictate the formation of singularities with or without event horizons [5].

Now a crucial question emerges: does a massive collapsing star conclude as a black hole or a naked singularity? This inquiry poses an ongoing challenge. To address this, understanding the physical and geometrical attributes of black holes and their alternatives is essential. As highlighted earlier, relatively realistic astrophysical scenarios can yield naked singularities, which may have substantial implications for our Universe's comprehension.

In principle, the theory of general relativity (GR) predicts that the spacetime singularity forms necessarily when large enough mass collapses under its own gravity. Nevertheless, it does not necessarily simultaneously enforce the formation (or otherwise) of an event horizon. In [5], Joshi, Malafarina, and Narayan have shown that a non-zero tangential pressure can prevent the formation of trapped surfaces around the core of a high-density region of a collapsing matter cloud, resulting in a central

* virajrk6@gmail.com

† grcollapse@gmail.com

‡ psjcosmos@gmail.com

naked singularity in large co-moving time. All the same, Janis, Newman, and Winicour obtained a minimally coupled mass-less scalar field solution of the Einstein field equations [6]. The subsequent observational aspects have been studied in JMN-1 and JNW spacetimes including shadows and accretion disk properties [8–14], relativistic orbits of S2 star [15–18], hot spot [19], energy extraction [20–22], echos and Quasi-Normal modes [23, 24], etc.

Recently, the Event Horizon Telescope (EHT) collaboration has announced a major breakthrough in the imaging of an ultra-compact object at the center of our galaxy [25]. While there is strong evidence that there is a massive concentration of mass in the center of our Milky Way galaxy, the question of whether or not it is a black hole with an event horizon is still open. The EHT shadow images of the M87 and Sgr A* do not explicitly prove the notion and existence of an event horizon. As it happens, other compact objects can as well cast similar shadows [26]. The JMN-1 and JNW spacetimes with a photon sphere maybe two of the best possible black hole mimickers for Sgr A* [5, 8–10]. Hence, the possibility that Sgr A* is a JMN-1 or JNW naked singularity cannot be ruled out based on the metric tests described in the EHT papers and they favourably acknowledged this fact [27]. Similarly, the shadows created by compact objects, including black holes, naked singularities, and also gravastars and wormholes, have received an attention [10, 11, 28–33].

These results piqued interest in the analysis of the nature of the object Sgr-A*. It has now become a subject of great interest to determine whether it is a supermassive black hole (SMBH) or a naked singularity. In this paper, we, therefore, have investigated the propagation time delay of pulsar signal in the vicinity of naked singularities.

The potential identification of pulsars in orbit around the SMBH at the center of the Milky Way provides a unique opportunity to test GR. Along with the timing analysis of the radio pulses emitted by these pulsars offers distinctive avenues for exploring the gravitational dynamics of the compact objects [34–38]. The implications of these observations on our current understanding of gravity are unparalleled, providing a unique opportunity to examine GR in the strong-field regime with exceptional precision. Additionally, it encourages rigorous investigation against alternative compact objects with remarkable accuracy. Because of its unparalleled potential to solve many mysteries of the universe, a large number

of radio pulsar searches had begun near the GC of the Milky Way galaxy [39–42]. Also, recent research suggests that there should be around 100 to 1000 pulsars orbiting within the range of 100 years of orbital period with an average of 100 pulsars in the range of 10 years orbit [35, 43–45]. This directs the search of pulsars in tight orbits around Sgr A*.

Even with considerable efforts, only six pulsars were detected within 15 arc-minutes of Sgr A* [41], and just one radio magnetar was detected at an angular distance of 2.4 arc-seconds from Sgr A* [46–48]. Due to the interstellar scattering process, which affects the temporal broadening of the pulses in a heavily turbulent and ionized interstellar medium at the GC [49], it is extremely hard to detect pulsars in tight orbit at the GC. The effectiveness of this procedure significantly relies on the observing frequency ν ($\propto \nu^4$), rendering the conventional periodicity search methods at frequencies around $\nu \sim 10GHz$ largely ineffective, even for pulsars with extended periods. The widening of pulse duration due to temporal broadening cannot be rectified or counteracted through instrumental adjustments or corrections [50]. To address this challenge, one potential approach is to shift pulsar searches to higher observing frequencies to reduce the scattering effect. However, considering the nature of pulsar spectra, which decrease flux density ($\propto \nu^\alpha$) as frequency increases (for $\alpha < 0$ as shown in [51]), higher frequencies correspond to fainter intrinsic source brightness.

Consequently, despite efforts, recent high-frequency pulsar searches in the GC, even using wavelengths of 2 and 3 mm [52], have failed to detect new pulsars in that area. Currently, new generation telescopes such as the Square Kilometre Array (SKA) [53], Five-hundred-meter Aperture Spherical Telescope (FAST) [54], the Event Horizon Telescope (EHT) [25] are actively searching for pulsars near Sgr A* and conducting time delay analyses. Hence, studying the time delay of light pulsations emitted by pulsars orbiting near the Milky Way GC is highly beneficial. Subsequently, we can evaluate how these time delays differ between black hole and horizon-less singularity spacetime models, aiding in the identification of the central compact object. This analysis will help us distinguish the Schwarzschild Black hole from JMN-1 and JNW naked singularities.

The paper is organised in the following manner. In Sec. II we define the methodology concerning the prop-

agation time delay of photon in Schwarzschild space-time which we compared with the time delay in post-Newtonian while in Sec. III we apply our methodology in JNW and JMN-1 spacetimes and find the core results of our analysis. In Sec. IV we discuss the results and their observational implications.

II. LIGHT PROPAGATION TIME IN SCHWARZSCHILD SPACETIME

The Schwarzschild metric in Boyer–Lindquist coordinates can be written as

$$ds^2 = -\left(1 - \frac{2M}{r}\right)(cdt)^2 + \left(1 - \frac{2M}{r}\right)^{-1} dr^2 + r^2(d\theta^2 + \sin^2\theta d\phi^2), \quad (1)$$

where $M = \frac{Gm}{c^2}$ and m is the mass of the black hole. The null geodesics along which photons propagate obey the geodesic equation

$$\ddot{x}^\mu + \Gamma_{\nu\rho}^\mu \dot{x}^\nu \dot{x}^\rho = 0, \quad (2)$$

where Γ denotes the Christoffel symbol, and the dot signifies the derivative with respect to the affine parameter τ along the curve. To retain the spherical symmetry of the spacetime, we set $\theta = \pi/2$ by considering the orbital plane as the equatorial plane. Consequently, we define the energy E and the angular momentum L as

$$E = g_{tt}(c\dot{x}^t) = -\left(1 - \frac{2M}{r}\right) \frac{cdt}{d\tau}, \quad (3)$$

$$L = g_{\phi\phi}\dot{\phi} = r^2 \frac{d\phi}{d\tau}, \quad (4)$$

also the condition for null geodesics,

$$g_{\mu\nu}\dot{x}^\mu \dot{x}^\nu = 0. \quad (5)$$

From Eqs. (3), (4), and (5) we can find the equations of motion for light,

$$\begin{aligned} \left(\frac{dr}{d\tau}\right)^2 &= \frac{1}{g_{rr}} \left(\frac{E^2}{g_{tt}} - \frac{L^2}{g_{rr}} \right) \\ &= \frac{L^2}{g_{rr}} \left(\frac{1}{b^2 g_{tt}} - \frac{1}{g_{\phi\phi}} \right) = L^2 R(r, b), \end{aligned} \quad (6)$$

$$\frac{d\phi}{d\tau} = \frac{L}{g_{\phi\phi}} = \frac{L}{r^2}, \quad (7)$$

$$\frac{cdt}{d\tau} = \frac{E}{g_{tt}} = \frac{E}{1 - \frac{2M}{r}}, \quad (8)$$

where, the impact parameter $b = L/E$ and

$$R(r, b) = \frac{1}{r^4} \left(\frac{r^4}{b^2} - r^2 + 2Mr \right). \quad (9)$$

To locate the turning point of the null geodesic, we set the component $dr/d\tau = 0$ and determine the roots of $R(r, b)$. The quartic polynomial $R(r, b)$ possesses four roots: one at zero and one as a negative root for all values of b . The other two roots vary based on the impact parameter b . When $b = b_{crit} = \sqrt{27}M$, these roots combine to yield a single positive root, indicating an unstable circular orbit. For $b > b_{crit}$, two positive roots emerge, resulting in either a flyby orbit (from infinity to the closest approach and then to the observer) or a terminating bound orbit. However, for $b < b_{crit}$, a complex pair arises, resulting in a terminating escaping orbit (from infinity and falls into the singularity at $r = 0$). [55].

Consider a pulsar orbiting the GC in a circular orbit as shown in Figure 1. Given the substantial mass distinction between the GC and the pulsar, the pulsar is treated as a test particle emitting radio pulses at different positions in the orbit shown as a circular long-dashed line. We are interested in finding the arrival time of the photons detected by an observer situated at a large distance r_0 . Therefore, we focus on the flyby orbit, where a photon emitted from the pulsar either reaches the observer directly shown by a red dashed line in Figure 1 or travels to the closest approach (r_{min}), the largest root of the polynomial in equation (9) before directed to the observer shown as a purple dashed line. The trajectory γ is contingent upon the pulsar's position. If the pulsar is in front of the GC from the observer's frame (P_1), it indicates direct propagation. Conversely, if the pulsar is behind the GC in the observer's frame (P_2), it signifies indirect propagation.

To determine the arrival time of the photon, we are required to solve the emitter-observer problem in order to find the impact parameter b of corresponding propagating photons determined as a grid of pulsar positions in the circular orbit. We also need to match direct and indirect propagation at the pulsar position P_3 in order to find the impact parameter. From equations of motion, we get

$$\frac{dr}{d\phi} = g_{\phi\phi} \sqrt{R(r, b)}, \quad (10)$$

$$\Delta\phi = \int_{\gamma} \frac{dr}{g_{\phi\phi} \sqrt{R(r, b)}}, \quad (11)$$

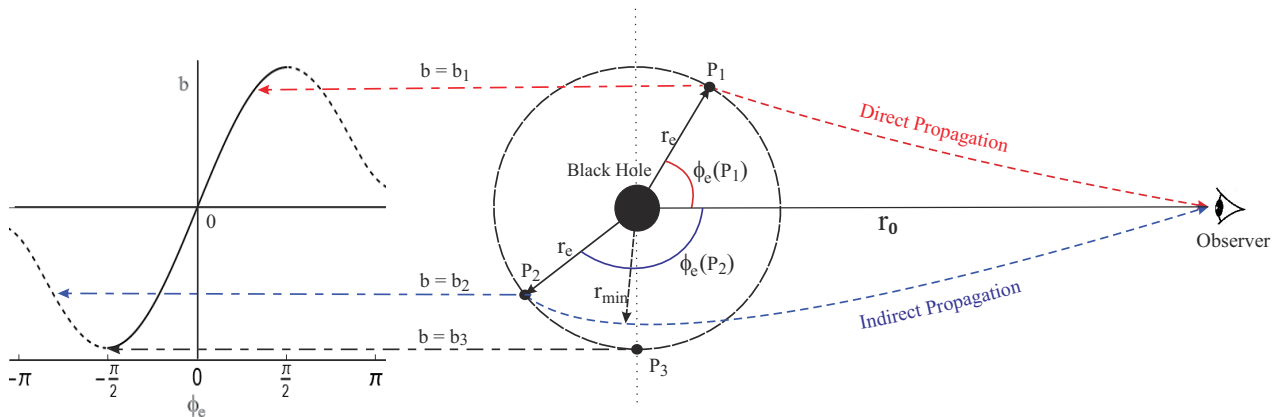


FIG. 1. A schematic diagram illustrating the emitter-observer problem for a circular orbit of the pulsar on the equatorial plane. Pulsar positions given by the polar coordinates (r_e, ϕ_e) are denoted by P_1 , P_2 , and P_3 for different positions in the orbit of a black hole at radius r_e shown by a long-dashed line. The observer is located at (r_o, ϕ_o) , where ϕ_o equals zero. The diagram shows direct (red dashed line) and indirect (purple dashed line) photon propagation scenarios, depicting how photons reach the observer from the pulsar. On the left side of the figure, photon impact parameter variations with pulsar positions are represented using a two-dashed arrow line on $(b \rightarrow \phi_e)$ plot.

where $\Delta\phi$ is the angle difference along the photon trajectory γ in the instantaneous common plane of pulsar and observer. There is no exact analytical solution to equation (11) is available. However, there is some literature in which authors have tried to approximate the analytical solution for the Schwarzschild black hole [56–58]. The approximation methods are not sufficient enough for our study, and hence we solve it completely numerically for both direct and indirect propagation. In direct propagation, the photon travels directly from r_e to r_o . On the other hand, in indirect propagation, the photon has to travel an additional distance. The photon first goes to the minimum approach and then to the observer ($r_e \rightarrow r_{min} \rightarrow r_o$). Hence, we are left with

$$\Delta\phi_d(SC) = \int_{r_e}^{r_o} \frac{dr}{r^2 \sqrt{R(r, b)}}, \quad (12)$$

$$\Delta\phi_{id}(SC) = \left[\int_{r_e}^{r_{min}} + \int_{r_{min}}^{r_o} \right] \frac{dr}{r^2 \sqrt{R(r, b)}}. \quad (13)$$

For this analysis, we consider Sgr-A* with the mass $M = 4 \times 10^6 M_\odot$ and $M_\odot = \frac{Gm_\odot}{c^2} = 1476\text{m}$, where m_\odot is mass of the sun, along with an Earth-based observer situated at a distance of approximately 8 kpc, equivalent to $4 \times 10^{10}\text{M}$ from the Sgr-A*. Assuming the pulsar

orbits in a circular path at a distance of 100M from the center. These conventions are taken from [55].

Also, we need to find the largest value of impact parameter b_{max} at the separation point $\pi/2$ and $-\pi/2$. We achieve this by finding the root of b in $dr/d\tau = 0$ at $r = r_e$. The emitter-observer problem is then solved numerically for equation (11).

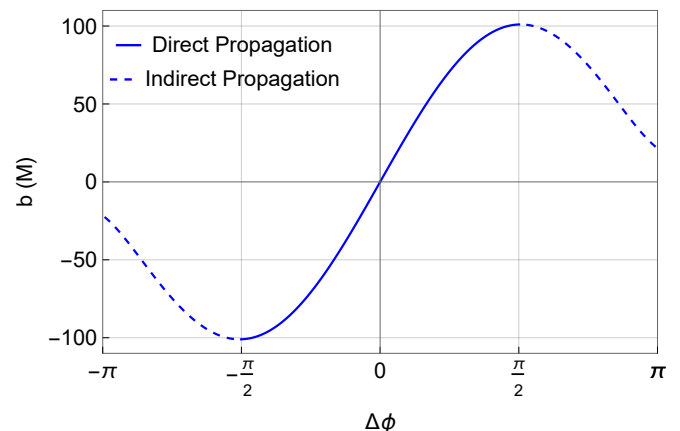


FIG. 2. Emitter-observer problem for Schwarzschild metric for a fixed observer located at $r_o = 8\text{kpc}$ in the range of $[0, 2\pi]$. The dashed line represents indirect propagation while the solid lines show direct propagation.

Figure 2 represents the solution of the emitter-observer problem. The separation point is slightly diverted from $\pi/2$ and $-\pi/2$ due to the strong gravitational lensing effect. For a sufficiently larger orbit, the separation is smaller, and vice versa.

Once we have the impact parameter (b) associated with the angle difference of photon between emission and observation ($\Delta\phi$), our focus shifts to determining the arrival time of photons. For simplicity, we initially disregard the gravitational field of the Sun, as well as the Earth's motion around it. Nonetheless, it's possible to incorporate these disregarded effects later by employing a weak field approximation for the Sun [59].

From equations of motion,

$$\frac{dt}{dr} = \frac{1/b}{g_{tt}\sqrt{R(r,b)}}, \quad (14)$$

$$\Delta t \equiv t_o - t_e = \int_{r_e, \gamma}^{r_o} \frac{1/b}{g_{tt}\sqrt{R(r,b)}} dr. \quad (15)$$

We again define two paths for photons to follow, direct and indirect corresponding to the solution of the position of the pulsar in the range of $[0, \pi]$. During 0 to $\pi/2$, the direct propagation is considered under the access of impact parameter solved from the emitter-observer problem. Similarly for $\pi/2$ to π , for indirect propagation,

$$\Delta t_d(SC) = \int_{r_e}^{r_o} \frac{1}{b(1 - \frac{2M}{r})\sqrt{R(r,b)}} dr, \quad (16)$$

$$\begin{aligned} \Delta t_{id}(SC) &= \int_{r_e}^{r_{min}} \frac{1}{b(1 - \frac{2M}{r})\sqrt{R(r,b)}} dr \\ &+ \int_{r_{min}}^{r_o} \frac{1}{b(1 - \frac{2M}{r})\sqrt{R(r,b)}} dr. \end{aligned} \quad (17)$$

The arrival time has no analytical solution available. However, in [55] the authors try to solve the integral for the Schwarzschild spacetime using the Jacobian elliptical integral to find the exact solution. Here, we solve the integral numerically and hence do not require the use of Jacobian elliptical functions.

Considering a Keplerian orbit of the pulsar (The assumption has no impact on our method for the fully relativistic solution), we have $r_e = \frac{a(1-e^2)}{1+e \cos \phi_e}$ where a is semi-major axis, e is eccentricity and ϕ_e is true anomaly. From [55] we adopt a toy model for our calculation with an inclination angle $i = \pi/3$ in a common plane along

with the argument of periastron $\omega = -\pi/2$. Therefore, the angle ϕ in equation (11), in the instantaneous common plane of pulsar and observer, is determined as

$$\cos \phi = -\sin i \times \sin(\omega + \phi_e). \quad (18)$$

Using equation (18) we can now find the true anomaly ϕ_e from the propagation angle ϕ in a common plane which is dependent on the impact parameter from the emitter-observer.

Now that we have the true anomaly of the pulsar's circular orbit as a function of the impact parameter, we can proceed to find the arrival time. Here we use a methodology in which we find the numerical value of the minimum approach at the grid of points between $[0, \pi]$ to describe the motion for direct and indirect propagation then interpolating all the discrete values in the arrival time formula. The whole arrival time problem is solved solely with the value of the impact parameter hence we define every function with only the impact parameter as a variable function including r_{min} . Also, to verify our methodology we subtract the R oemer time and Shapiro time from the derived Schwarzschild expression according to [55]. Here, note that we define the reference point at $\pi/2$.

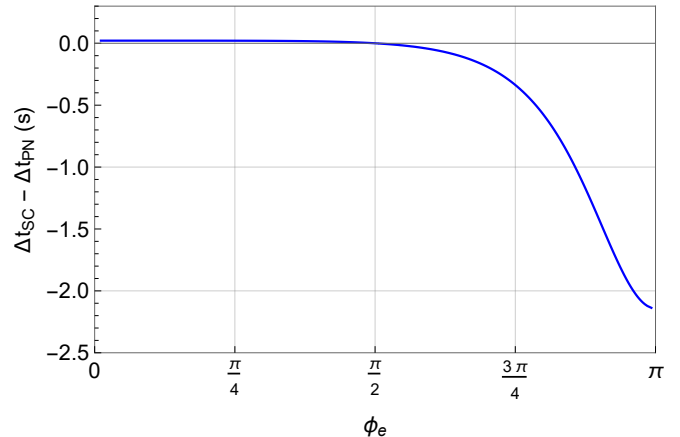


FIG. 3. Time delay difference in Schwarzschild spacetime and post-Newtonian approach in seconds from 0 to π for the toy model considered using direct and indirect propagation formulas.

In Figure 3, we calculated the time delay discrepancy between Schwarzschild and post-Newtonian, which is already explored in [55] to validate our approach. We can see that during direct propagation, at $\phi_e = 0$ the time delay is 21.4 ms, however, the main difference can be seen

in indirect propagation, where the difference is -2.137 s at $\phi_e = \pi$. This verifies our results by matching the analysis carried out in [55].

III. PROPAGATION TIME DELAY IN NAKED SINGULARITIES

After formulating the methodology of finding the time delay in Schwarzschild spacetime we can use the same formulation for alternative spacetimes as well. In [60] authors have derived the time delay difference between the Schwarzschild and its alternative black hole spacetimes. As the behaviour of the spacetime metric affects the null geodesics we now apply the formulation to find the arrival time in naked singularity spacetimes and compare it with the Schwarzschild spacetime. The naked singularity is a horizonless singularity from which the past incomplete null geodesics can exit from the singularity. There are two naked singularity models we have considered in this paper as follows.

A. Janis-Newman-Winicour Spacetime

The first spacetime we studied was given by Janis, Newman, and Winicour in 1968 [6] with a massless scalar field. The JNW solution satisfies the weak energy condition and has a strong globally naked singularity [61]. The metric of JNW can be written as

$$ds^2 = -\left(1 - \frac{2\mathcal{M}}{r}\right)^\gamma dt^2 + \left(1 - \frac{2\mathcal{M}}{r}\right)^{-\gamma} dr^2 + \left(1 - \frac{2\mathcal{M}}{r}\right)^{1-\gamma} r^2 d\Omega^2, \quad (19)$$

with $d\Omega^2 = d\theta^2 + \sin^2\theta d\phi^2$ and associated scalar field,

$$\Phi(r) = \frac{\sqrt{1-\gamma^2}}{2} \ln\left(1 - \frac{2\mathcal{M}}{r}\right) \quad (20)$$

$$= \frac{q}{2\mathcal{M}} \ln\left(1 - \frac{2\mathcal{M}}{r}\right), \quad (21)$$

where \mathcal{M} is related to the ADM mass M of the compact object which can be defined as

$$\mathcal{M} = \sqrt{M^2 + q^2}, \quad \gamma = \frac{M}{\mathcal{M}}, \quad (22)$$

with two free parameters, the ADM mass M of the gravitational compact object and the scalar charge q . The

scalar charge can be defined as

$$q = M \left(\frac{1 - \gamma^2}{\gamma^2} \right), \quad (23)$$

with $0 < \gamma < 1$. We can obtain the Schwarzschild solution just by putting $q = 0$ in equation (19). For simplicity, we take the equatorial plan, hence, $\theta = \pi/2$ and $\phi = 0$. Using the condition of null geodesics from equation (5), we can find the equations of motion for photon in the JNW metric.

$$\left(\frac{dr}{d\tau}\right)^2 = L^2 \left[\frac{1}{b^2} - \frac{1}{\left(1 - \frac{2\mathcal{M}}{r}\right)^{1-2\gamma} r^2} \right] \quad (24)$$

$$= L^2 R_{JNW}(r, b),$$

$$\frac{d\phi}{d\tau} = \frac{L}{g_{\phi\phi}} = \frac{L}{\left(1 - \frac{2\mathcal{M}}{r}\right)^{1-\gamma} r^2}, \quad (25)$$

$$\frac{cdt}{d\tau} = \frac{E}{g_{tt}} = \frac{E}{\left(1 - \frac{2\mathcal{M}}{r}\right)^\gamma}. \quad (26)$$

We solve the largest root of $R_{JNW}(r, b)$ for different values of impact parameter b and specific value of scalar charge q . For the JNW case, we use the same approach shown in Figure 1. Here, instead of a black hole at the center, we have a naked singularity and solve the emitter-observer problem from equation (11).

$$\Delta\phi_{JNW} = \int_{\gamma} \frac{dr}{\left(1 - \frac{2\mathcal{M}}{r}\right)^{1-\gamma} r^2 \sqrt{R_{JNW}(r, b)}}. \quad (27)$$

In this equation, we take different paths according to the direct and indirect propagation and solve the emitter-observer problem.

After solving the emitter-observer problem as a function of impact factor b we now move forward to find the arrival time for direct as well indirect propagation for the JNW using equation (15).

$$\Delta t_d(JNW) = \int_{r_e}^{r_0} \frac{dr}{b \left(1 - \frac{2\mathcal{M}}{r}\right)^\gamma \sqrt{R_{JNW}(r, b)}}, \quad (28)$$

$$\Delta t_{id}(JNW) = \int_{r_e}^{r_{min}} \frac{dr}{b \left(1 - \frac{2\mathcal{M}}{r}\right)^\gamma \sqrt{R_{JNW}(r, b)}} + \int_{r_{min}}^{r_0} \frac{dr}{b \left(1 - \frac{2\mathcal{M}}{r}\right)^\gamma \sqrt{R_{JNW}(r, b)}}. \quad (29)$$

In Figure 5 we examine the time delay of radio pulses in JNW spacetime for a pulsar in a circular orbit in comparison with the Schwarzschild black hole. The scalar charge takes values between 0 M and 1 M . As shown in

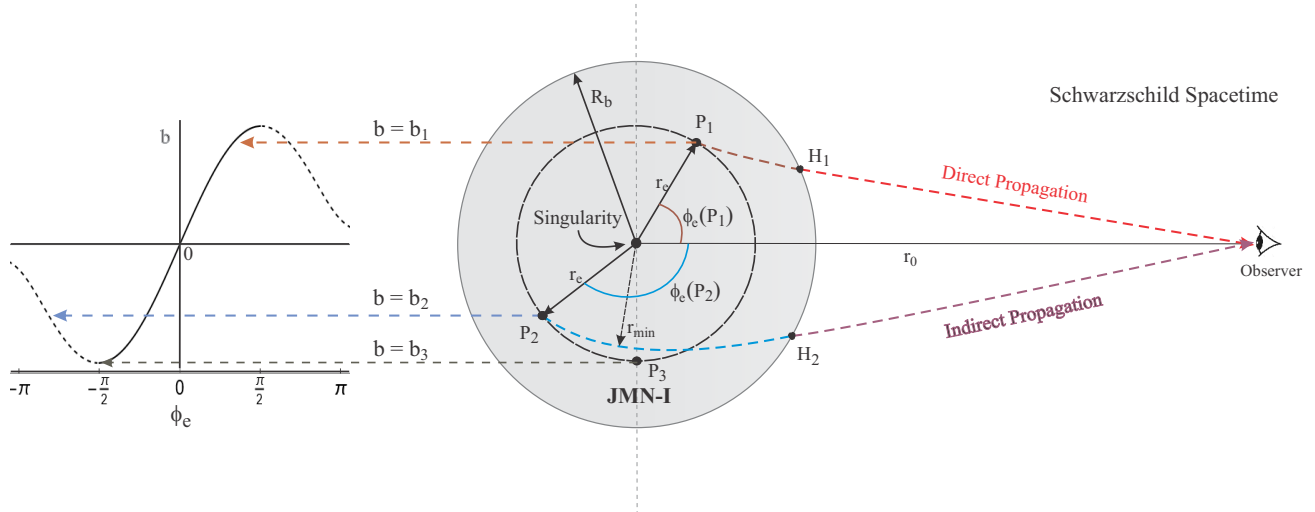


FIG. 4. The figure illustrates the emitter-observer problem in JMN-1 spacetime. The JMN-1 spacetime is enclosed inside of the R_b radius (shaded portion) with a singularity at the center and outside is the Schwarzschild spacetime with matching at R_b . The pulsar orbit (long-dashed line) is inside of the JNW-1 spacetime. In the photon paths, we also matched both spacetimes at points denoted by H_1 and H_2 for direct (brown and red dashed line) and indirect (blue and purple dashed line) propagation respectively. The left side of the figure shows the impact parameter for the photon corresponding the pulsar position (r_e, ϕ_e) shown by a two-dashed arrow line indicating on $(b \rightarrow \phi_e)$ plot.

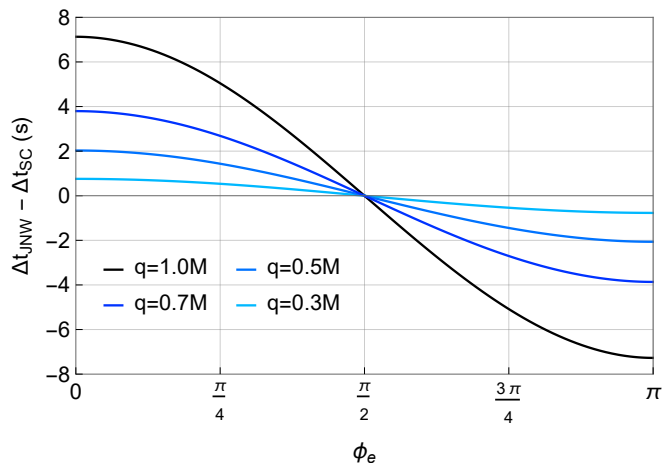


FIG. 5. The time delay in JNW naked singularity in comparison with the Schwarzschild black hole for the different values of scalar charge (q). The considered mass of central object Sgr-A* is $M = 4 \times 10^6 M_\odot$. While the pulsar is in the $r_e = 100M$ circular inclined orbit at $i = \pi/3$ with the earth-based observer at $r_0 = 8kpc$ from the GC.

Figure 5, for $q = 1 M$ (indicated by the solid black line), the time delay when compared to Schwarzschild reaches up to -7.27 s at $\phi_e = \pi$, whereas at $\phi_e = 0$ the dif-

ference is 7.13 s which is total of 14.40s. We analysed that a smaller scalar charge yields a closer match to the Schwarzschild model.

B. Joshi-Malafarina-Narayan Spacetime

The second spacetime we use was given by Joshi, Malafarina, and Narayan [5] which is a result of an inhomogeneous dust collapse and a better alternative to the OSD collapse [1, 2] as the OSD collapse model assumes an idealistic set of initial conditions for a homogeneous dust collapse. The solution holds a time-like naked singularity at $r = 0$ and does not allow the formation of trapped surfaces. The metric is given by

$$ds^2 = -(1-M_0) \left(\frac{r}{R_b} \right)^{\frac{M_0}{1-M_0}} dt^2 + \left(\frac{1}{1-M_0} \right) dr^2 + r^2 d\Omega^2, \quad (30)$$

where the parameter M_0 is in the range $0 \leq M_0 \leq 4/5$. The total mass M is given by $M = \frac{1}{2} M_0 R_b$. The metric is naturally matching with the Schwarzschild at an outer radius at $r = R_b$.

From null geodesics, we get the following equations of

motion

$$\left(\frac{dr}{d\tau}\right)^2 = L^2 \left[\frac{1}{b^2} \left(\frac{R_b}{r}\right)^{\frac{M_0}{1-M_0}} - \frac{1-M_0}{r^2} \right] \quad (31)$$

$$= L^2 R_{JMN}(r, b),$$

$$\frac{d\phi}{d\tau} = \frac{L}{r^2}, \quad (32)$$

$$\frac{cdt}{d\tau} = \frac{E}{1-M_0} \left(\frac{R_b}{r}\right)^{\frac{M_0}{1-M_0}}. \quad (33)$$

We again solve the emitter-observer problem which is shown in Figure 4 using equation (11) for JMN-1 and find the angle difference between the emission of the photon from a pulsar path and the observer at the Earth which we later connect with the impact parameter using the following equation derived from equations of motion

$$\Delta\phi(JMN) = \int_{\gamma} \frac{dr}{r^2 \sqrt{R_{JMN}(r, b)}}. \quad (34)$$

Since JMN-1 is not asymptotically flat, we considered the JMN-1 as interior spacetime inside the radius R_b and the pulsar orbit within the sphere $0 < r_e < R_b$. Outside of the sphere, the exterior Schwarzschild spacetime is matched for asymptotic flatness at large distances where an Earth-based observer is placed. Hence, it is required to match the null geodesics path for JMN-1 and Schwarzschild spacetime at $r = R_b$. To properly match the spacetimes we need to match the impact parameters of both spacetimes. Hence we match $R(r, b)$ for different values of r and find b for Schwarzschild which we now denote as b_{sc} . The time delay can be found from

$$\Delta t_d(JMN) = \int_{r_e}^{R_b} \frac{(R_b/r)^{(M_0/1-M_0)} dr}{b(1-M_0)\sqrt{R_{JMN}(r, b)}} + \int_{R_b}^{r_o} \frac{dr}{b_{sc}(1-\frac{2M}{r})\sqrt{R_{sc}(r, b_{sc})}}, \quad (35)$$

$$\Delta t_d(JMN) = \int_{r_e}^{r_{min}} \frac{(R_b/r)^{(M_0/1-M_0)} dr}{b(1-M_0)\sqrt{R_{JMN}(r, b)}} + \int_{r_{min}}^{R_b} \frac{(R_b/r)^{(M_0/1-M_0)} dr}{b(1-M_0)\sqrt{R_{JMN}(r, b)}} + \int_{R_b}^{r_o} \frac{dr}{b_{sc}(1-\frac{2M}{r})\sqrt{R_{sc}(r, b_{sc})}}. \quad (36)$$

As shown in Figure 6 we assume different values of model parameters to find out the time delay in JMN-1 in comparison to Schwarzschild. We used three different

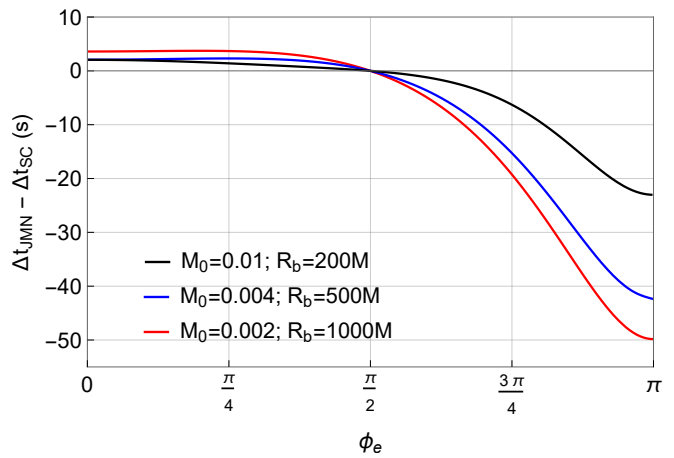


FIG. 6. The time delay in JMN-1 compared with the Schwarzschild for the different model parameters M_0 and R_b . The mass of the GC, circular pulsar orbit radius and inclination is $M = 4 \times 10^6 M_\odot$, $r_e = 100M$, and $i = \pi/3$ respectively. Where model parameter R_b value is always larger than the pulsar orbit. In the region of $R_b < r < r_o$, the Schwarzschild metric is considered to achieve the asymptotic flatness for the earth-based observer.

values of the model parameter M_0 and found the difference. It can be observed that when $M_0 = 0.002$, which corresponds to $R_b = 1000M$, we find a very large time difference. At $\phi_e = \pi$, the propagation time delay difference is almost -50 s. On the other hand, at $\phi_e = 0$, we get only ~ 3.6 s. We observe that as more photons traverse through JMN-1 spacetime, the smaller the propagation time delay difference with the Schwarzschild black hole during indirect propagation. Conversely, in direct propagation, photons take more time in propagation compared to the Schwarzschild black hole.

IV. RESULTS AND DISCUSSION

Studying radio pulses generated by the pulsar in the proximity of the GC is the main motivation for this study. Observationally detecting a pulsar in a tight orbit of GC can open up unprecedented opportunities for studying extreme gravity physics, testing GR, and understanding the nature of the compact object.

In this work, we numerically measured the propagation time delay of photons generated by the pulsar in a circular orbit in various spacetimes assuming the source to be Sgr-A*, with mass $M = 4 \times 10^6 M_\odot$ and Earth-based observer at a distance of $r_o = 8kpc$. We first

solved the geodesic equations of propagating photons to consider all the GR effects and numerically solved the emitter-observer problem shown in Fig. (2). Once we get access to the impact parameter from the emitter-observer, we find the time delay in Schwarzschild. The post-Newtonian approximation is considered in Fig. (3) to quantify GR effects on the photons' trajectories. The time delay difference is measured to be -2.137 s during the indirect proportion $\phi_e = \pi$. On the other hand, during the direct propagation, the delay difference is comparably very small around 21.4 ms at $\phi_e = 0$.

The same formulation is then applied to JNW spacetime and compared with the Schwarzschild which is shown in Figure 5. We analyzed that the scalar charge is impacting largely on the behavior of photon propagation. For larger values of scalar charge ($q = 1$ M) the measured time delay difference is very large. During direct propagation, the photon propagation in JNW takes approximately 7.13 s more compared to the Schwarzschild black hole at $\phi_e = 0$. On the other hand, during the indirect propagation, photon traveling in JNW spacetime would take 7.27 s less at $\phi_e = \pi$. Besides, in more realistic cases the massless scalar field would have a very small value of ' q ' derived in [15], indicating an extremely small difference in time delay. On the contrary, JMN-1 spacetime is not asymptotically flat. Hence we considered a sphere of a certain radius (R_b) which has JMN-1 spacetime inside of it and outside is the Schwarzschild spacetime. To determine the time delay in JMN-1 spacetime, the orbit of the pulsar is considered inside the JMN-1 spacetime. We find out in Figure 6 that the time delay difference is larger as compared to Schwarzschild and increases even more for

a smaller value of M_0 (corresponding to a larger value of R_b). Besides, when the largest value of $M_0 = 0.01$ is considered ($R_b = 200$ M), the time delay difference is very notable. At $\phi_e = 0$, it is measured to be around 2 s and at $\phi_e = \pi$ it is -23 s which extends up to -50 s for very small value of $M_0 = 0.02$ at $\phi_e = \pi$ while at $\phi_e = 0$ it is 3.6 s.

The future prospects of pulsar research are very promising and multifaceted. Pulsars' unique properties make them invaluable laboratories for studying stellar and binary evolution, as well as probing GR at a fundamental level. Advanced surveys like SKA, and EHT of pulsars studies will revolutionize our understanding of fundamental physics. Recently, in a search of pulsars at our Milky Way GC, the EHT used 2017 observation data from its three most sensitive telescopes, the Atacama Large Millimeter/submillimeter Array, the Large Millimeter Telescope and the IRAM 30m Telescope but they did not find any significant pulsar signal due to insufficient sensitivity to detect pulsars [62]. Despite initial challenges, ongoing advancements in technology and methodology with modified frequency searches specific for pulsar detection promise to unveil a wealth of new knowledge, transforming our understanding of pulsars.

Furthermore, the highly sensitive SKA survey will greatly enhance the accuracy of timing measurements for millisecond pulsars which will be helpful to test GR in ways not possible before [63]. Also, the discovery of relativistic pulsar systems, potentially including pulsar-black hole binaries, holds the key to unraveling cosmic mysteries such as the cosmic censorship conjecture and the no-hair theorem.

-
- [1] J. R. Oppenheimer and H. Snyder, *Phys. Rev.* **56**, 455-459 (1939)
 - [2] B. Datt, *Zeitschrift fur Physik* **108**, 5-6, 314-321 (1938).
 - [3] R. Penrose, *Riv. Nuovo Cim.* **1**, 252-276 (1969).
 - [4] P. S. Joshi and I. H. Dwivedi, *Phys. Rev. D* **47**, 5357-5369 (1993).
 - [5] P. S. Joshi, D. Malafarina and R. Narayan, *Class. Quant. Grav.* **28**, 235018 (2011).
 - [6] A. I. Janis, E. T. Newman, J. Winicour, *Phys. Rev. Lett.* **20**, 878-880 (1968).
 - [7] V. Perlick, *Classical and Quantum Gravity*, **9**, 4, 1009-1021 (1992).
 - [8] Saurabh, P. Bambhaniya and P. S. Joshi, *A & A* **628** A113, 8, (2024).
 - [9] Saurabh, P. Bambhaniya and P. S. Joshi, [arXiv:2202.00588](https://arxiv.org/abs/2202.00588) [gr-qc].
 - [10] R. Shaikh, P. Kocherlakota, R. Narayan and P. S. Joshi, *Mon. Not. Roy. Astron. Soc.* **482**, no.1, 52-64 (2019).
 - [11] G. Gylulchev, P. Nedkova, T. Vetsov and S. Yazadjiev, *Phys. Rev. D* **100**, no.2, 024055 (2019).
 - [12] D. N. Solanki, P. Bambhaniya, D. Dey, P. S. Joshi and K. N. Pathak, *Eur. Phys. J. C* **82**, no.1, 77 (2022).
 - [13] S. Sau, I. Banerjee and S. SenGupta, *Phys. Rev. D* **102**, no.6, 064027 (2020).
 - [14] A. N. Chowdhury, M. Patil, D. Malafarina and P. S. Joshi, *Phys. Rev. D* **85**, 104031 (2012).

- [15] P. Bambhaniya, A. B. Joshi, D. Dey, P. S. Joshi, A. Mazumdar, T. Harada and K. i. Nakao, *Eur. Phys. J. C* **84**, no.2, 124 (2024).
- [16] P. Bambhaniya, A. B. Joshi, D. Dey and P. S. Joshi, *Phys. Rev. D* **100**, no.12, 124020 (2019).
- [17] A. B. Joshi, P. Bambhaniya, D. Dey and P. S. Joshi, [arXiv:1909.08873 \[gr-qc\]](https://arxiv.org/abs/1909.08873).
- [18] D. Dey, P. S. Joshi, A. Joshi and P. Bambhaniya, *Int. J. Mod. Phys. D* **28**, no.14, 1930024 (2019).
- [19] Y. Chen, P. Wang and H. Yang, [arXiv:2309.04157 \[gr-qc\]](https://arxiv.org/abs/2309.04157).
- [20] V. Patel, K. Acharya, P. Bambhaniya and P. S. Joshi, *Universe* **8**, no.11, 571 (2022).
- [21] V. Patel, K. Acharya, P. Bambhaniya and P. S. Joshi, *Phys. Rev. D* **107**, no.6, 064036 (2023).
- [22] K. Acharya, K. Pandey, P. Bambhaniya, P. S. Joshi and V. Patel, [arXiv:2303.16590 \[gr-qc\]](https://arxiv.org/abs/2303.16590).
- [23] A. Chowdhury and N. Banerjee, *Phys. Rev. D* **102**, no.12, 124051 (2020).
- [24] O. S. Stashko, O. V. Savchuk and V. I. Zhdanov, *Phys. Rev. D* **109**, no.2, 024012 (2024).
- [25] K. Akiyama *et al.* [Event Horizon Telescope], *Astrophys. J. Lett.* **930**, no.2, L12 (2022).
- [26] S. Vagnozzi, R. Roy, Y. D. Tsai, L. Visinelli, M. Afrin, A. Allahyari, P. Bambhaniya, D. Dey, S. G. Ghosh and P. S. Joshi, *et al. Class. Quant. Grav.* **40**, no.16, 165007 (2023).
- [27] K. Akiyama *et al.* [Event Horizon Telescope], *Astrophys. J. Lett.* **930**, no.2, L17 (2022).
- [28] T. Ohgami and N. Sakai, *Phys. Rev. D* **91**, no.12, 124020 (2015).
- [29] N. Sakai, H. Saida and T. Tamaki, *Phys. Rev. D* **90**, no.10, 104013 (2014).
- [30] P. Bambhaniya, S. K. K. Jusufi and P. S. Joshi, *Phys. Rev. D* **105**, no.2, 023021 (2022).
- [31] V. Vertogradov, P. Bambhaniya and M. Misyura, [arXiv:2403.16743 \[gr-qc\]](https://arxiv.org/abs/2403.16743).
- [32] P. Bambhaniya, D. Dey, A. B. Joshi, P. S. Joshi, D. N. Solanki and A. Mehta, *Phys. Rev. D* **103**, no.8, 084005 (2021).
- [33] A. B. Joshi, D. Dey, P. S. Joshi and P. Bambhaniya, *Phys. Rev. D* **102**, no.2, 024022 (2020).
- [34] N. Wex and S. Kopeikin, *Astrophys. J.* **514**, 388 (1999).
- [35] E. Pfahl and A. Loeb, *Astrophys. J.* **615**, 253-258 (2004).
- [36] M. Kramer, D. C. Backer, J. M. Cordes, T. J. W. Lazio, B. W. Stappers and S. Johnston, *New Astron. Rev.* **48**, 993-1002 (2004).
- [37] D. Psaltis, N. Wex and M. Kramer, *Astrophys. J.* **818**, no.2, 121 (2016).
- [38] K. Liu, N. Wex, M. Kramer, J. M. Cordes and T. J. W. Lazio, *Astrophys. J.* **747**, 1 (2012).
- [39] S. Johnston, M. A. Walker, M. H. Van Kerkwijk and A. G. Lyne, *Mon. Not. Roy. Astron. Soc.* **274**, 1, L43-L45 (1995).
- [40] S. Johnston, M. Kramer, D. R. Lorimer, A. G. Lyne, M. McLaughlin, B. Klein and R. N. Manchester, *Mon. Not. Roy. Astron. Soc.* **373**, L6-L10 (2006).
- [41] J. S. Deneva, J. M. Cordes and T. J. W. Lazio, *Astrophys. J. Lett.* **702**, L177-L181 (2009).
- [42] S. D. Bates, S. Johnston, D. R. Lorimer, M. Kramer, A. Possenti, M. Burgay, B. Stappers, M. J. Keith, A. Lyne and M. Bailes, *et al. Mon. Not. Roy. Astron. Soc.* **411**, 1575 (2011).
- [43] F. Zhang, Y. Lu and Q. Yu, *Astrophys. J.* **784**, 106 (2014).
- [44] K. Rajwade, D. Lorimer and L. Anderson, *Mon. Not. Roy. Astron. Soc.* **471**, no.1, 730-739 (2017).
- [45] J. Chennamangalam and D. R. Lorimer, *Mon. Not. Roy. Astron. Soc.* **440**, 86 (2014).
- [46] J. A. Kennea, D. N. Burrows, C. Kouveliotou, D. M. Palmer, E. Gogus, Y. Kaneko, P. A. Evans, N. Degenaar, M. Reynolds and J. M. Miller, *et al. Astrophys. J. Lett.* **770**, L24 (2013).
- [47] K. Mori, E. V. Gotthelf, S. Zhang, H. An, F. K. Baganoff, N. M. Barriere, A. Beloborodov, S. E. Boggs, F. E. Christensen and W. W. Craig, *et al. Astrophys. J. Lett.* **770**, L23 (2013).
- [48] N. Rea, P. Esposito, J. A. Pons, R. Turolla, D. F. Torres, G. L. Israel, A. Possenti, M. Burgay, D. Viganò and R. Perna, *et al. Astrophys. J. Lett.* **775**, L34 (2013).
- [49] J. M. Cordes and T. J. W. Lazio, [[arXiv:astro-ph/0207156 \[astro-ph\]](https://arxiv.org/abs/astro-ph/0207156)].
- [50] R. P. Eatough, M. Kramer, B. Klein, R. Karuppusamy, D. J. Champion, P. C. C. Freire, N. Wex and K. Liu, *IAU Symp.* **291**, 382-384 (2013).
- [51] R. S. Wharton, S. Chatterjee, J. M. Cordes, J. S. Deneva and T. J. W. Lazio, *Astrophys. J.* **753**, 108 (2012).
- [52] P. Torne, G. Desvignes, R. Eatough, M. Kramer, R. Karuppusamy, K. Liu, A. Noutsos, R. Wharton, C. Kramer and S. Navarro, *et al. Astron. Astrophys.* **650**, A95 (2021).
- [53] E. F. Keane, B. Bhattacharyya, M. Kramer, B. W. Stappers, S. D. Bates, M. Burgay, S. Chatterjee, D. J. Champion, R. P. Eatough and J. W. T. Hessels, *et al. PoS AASKA14*, 040 (2015).
- [54] R. Nan, D. Li, C. Jin, Q. Wang, L. Zhu, W. Zhu, H. Zhang, Y. Yue and L. Qian, *Int. J. Mod. Phys. D* **20**, 989-1024 (2011).
- [55] E. Hackmann and A. Dhani, *Gen. Rel. Grav.* **51**, 3, 37 (2019).
- [56] O. Semerák, *Astrophys. J.* **800**, no.1, 77 (2015).
- [57] A. M. Beloborodov, *Astrophys. J. Lett.* **566**, L85-L88 (2002).

- [58] V. De Falco, M. Falanga and L. Stella, *Astron. Astrophys.* **595**, A38 (2016).
- [59] T. Damour and N. Deruelle, *AIHPA.* **44**, 3, 263-292 (1986).
- [60] R. Della Monica, I. de Martino and M. de Laurentis, *Mon. Not. Roy. Astron. Soc.* **524**, no.3, 3782-3796 (2023).
- [61] K. S. Virbhadra, S. Jhingan and P. S. Joshi, *Int. J. Mod. Phys. D* **6**, 357-362 (1997).
- [62] P. Torne *et al.* [EHT], *Astrophys. J.* **959**, no.1, 14 (2023).
- [63] L. Shao, I. H. Stairs, J. Antoniadis, A. T. Deller, P. C. C. Freire, J. W. T. Hessels, G. H. Janssen, M. Kramer, J. Kunz and C. Lämmerzahl, *et al.* *PoS AASKA14*, 042 (2015).